

## Electron-Phonon Interactions in Graphene, Bilayer Graphene, and Graphite

CheolHwan Park,<sup>1,2</sup> Feliciano Giustino<sup>1,2</sup> Marvin L. Cohen,<sup>1,2</sup> and Steven G. Louie<sup>1,2</sup><sup>1</sup>Department of Physics, University of California at Berkeley, Berkeley, California 94720, USA<sup>2</sup>Materials Sciences Division, Lawrence Berkeley National Laboratory, Berkeley, California 94720, USA

(Dated: February 21, 2024)

Using first-principles techniques, we calculate the renormalization of the electron Fermi velocity and the vibrational lifetimes arising from electron-phonon interactions in doped bilayer graphene and in graphite and compare the results with the corresponding quantities in graphene. For similar levels of doping, the Fermi velocity renormalization in bilayer graphene and in graphite is found to be approximately 30% larger than that in graphene. In the case of bilayer graphene, this difference is shown to arise from the interlayer interaction. We discuss our findings in the light of recent photoemission and Raman spectroscopy experiments.

Since the fabrication of crystalline graphite films with a thickness of only a few atoms<sup>1,2,3,4,5</sup>, single- and double-layer graphene have received considerable attention<sup>6</sup>. These materials are promising candidates for nanoelectronics applications because of the high mobility of charge carriers in these systems and the tunability of their electronic properties by gating<sup>6</sup>. Since electron-phonon (e-ph) interaction plays an important role in the dynamics of charge carriers<sup>7,8</sup>, understanding its effects in single- and double-layer graphene is of crucial importance for graphene-based electronics.

The e-ph interaction in metals modifies the dynamics of electrons with energy near the Fermi level by increasing their mass and reducing their lifetime. The mass renormalization can be described in terms of the e-ph coupling strength  $\gamma_{nk}$ , defined as the energy derivative of the real part of the phonon-induced electronic self-energy  $\gamma_{nk}(E)$  at the Fermi level  $E_F$ :  $\gamma_{nk} = \partial \text{Re } \gamma_{nk}(E) / \partial E|_{E=E_F}$ , where  $n$ ,  $k$  and  $E$  are the band index, the wavevector and the energy of the electron, respectively<sup>8</sup>. The electron mass renormalization can be obtained from the e-ph coupling strength through  $m = m_0(1 + \gamma_{nk})$  where  $m_0$  and  $m$  are the bare band mass and the renormalized mass, respectively. The e-ph interaction also gives rise to a phonon lifetime  $\tau_q = \hbar / \gamma_q$ , where  $\gamma_q$  is the phonon linewidth, i.e., twice the imaginary part of the phonon self-energy arising from the e-ph interaction. Here,  $q$  and  $\gamma_q$  are the phonon branch index, the wavevector and the energy of the phonon, respectively<sup>8</sup>.

These quantities can be calculated from first-principles within the Migdal approximation as<sup>8</sup>

$$\gamma_{nk} = \sum_{m; q} \frac{d\gamma}{dE} \gamma_{mn; (k;q)}^2 \left[ \frac{n_q + 1}{(E_F - \epsilon_{mk+q} - \epsilon_q)^2} + \frac{n_q + \epsilon_{mk+q} - \epsilon_q}{(E_F - \epsilon_{mk+q} + \epsilon_q)^2} \right] \quad (1)$$

and

$$\gamma_q = 4 \sum_{m, n} \frac{d\gamma}{dE} \gamma_{mn; (k;q)}^2 (\epsilon_{nk} - \epsilon_{mk+q}) (\epsilon_{mk+q} - \epsilon_{nk} - \epsilon_q) \quad (2)$$

Here  $\epsilon_{nk}$  and  $\epsilon_q$  are the energy eigenvalue of an elec-

tron with band index  $n$  and wavevector  $k$  and that of a phonon with branch index  $q$  and wavevector  $q$ , respectively.  $A_{BZ}$  is the area of the first Brillouin zone where the integration is performed. The quantities  $f_{nk}$  and  $n_q$  are the Fermi-Dirac and the Bose-Einstein factors, respectively, and  $\gamma_{mn; (k;q)} = \langle \psi_{mk+q} | V_q(r) | \psi_{nk} \rangle$  is the scattering amplitude of an electronic state  $\psi_{nk}$  into another state  $\psi_{mk+q}$  resulting from the change in the self-consistent field potential  $V_q(r)$  arising from a phonon with the branch index  $q$  and the wavevector  $q$ .

Electron wavefunctions and energy eigenvalues are obtained using *ab initio* pseudopotential density functional theory calculations<sup>10</sup> within the local density approximation<sup>11,12</sup>. Phonon frequencies and eigenstates are obtained through density functional perturbation theory<sup>13</sup>. We have used a plane wave basis set<sup>14</sup> with a kinetic energy cutoff of 60 Ry. The core-valence interaction is handled using norm-conserving pseudopotentials<sup>15,16</sup>. The integration in Eq. (1) for graphene and bilayer graphene is performed by summation over 300  $\times$  300 points and for graphite it is performed with 90  $\times$  90  $\times$  30 points in the irreducible part of the Brillouin zone. The integration of Eq. (2) for graphene and bilayer graphene is done by summation over 1000  $\times$  1000 points in the irreducible part of the Brillouin zone, and the function is replaced by a Lorentzian with 15 meV broadening for convergence. Electron and phonon wavefunctions, energy eigenvalues and the e-ph coupling matrix elements in these extremely dense grid sets are obtained by a recently developed interpolation scheme<sup>17,18</sup> based on maximally localized Wannier functions<sup>19,20</sup>. The Fermi-Dirac and Bose-Einstein factors are evaluated at the temperature  $T = 15$  K in all the calculations. Charge doping is modelled by adding or removing electrons from the simulation cell and by using a neutralizing background. In this work we assume that the layers in bilayer graphene and in graphite are arranged according to the Bernal stacking sequence [Fig. 1(a)]<sup>21</sup>.

Figure 1 shows the e-ph coupling strengths  $\gamma_{nk}$  in graphene, bilayer graphene and in graphite calculated along the reciprocal space path indicated by the double-headed arrow in Fig. 1(b). As pointed out in Ref.<sup>22</sup> the e-ph coupling strength in graphene  $\gamma_{nk}$  is insensitive to the

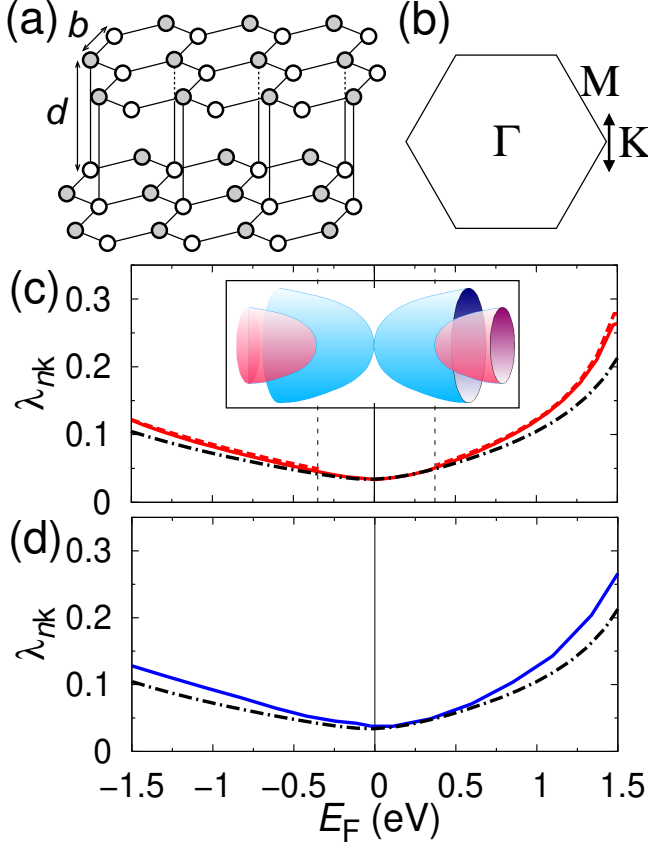


FIG. 1: (a) Ball-and-stick model of bilayer graphene (Bernal stacking). (b) Brillouin zone of graphene and bilayer graphene. (c) The electron-phonon coupling strength  $\lambda_{nk}$  in bilayer graphene versus changing Fermi level  $E_F$  calculated along the path (double-head arrow) shown in (b). Solid and dashed red lines correspond to  $\lambda_{nk}$  of the individual blue and red parabolic band in the inset, respectively. The Fermi level of neutral bilayer graphene is set at zero. (d) As in (c), for each of the two electronic bands of graphite touching at the  $K$  point (solid blue line). In (c) and (d), we show for comparison the e-ph coupling strength in graphene<sup>22</sup> (indicated by the dash-dotted line).

location of the wavevector  $k$  on the Fermi surface. This is also the case for bilayer graphene and for graphite. Therefore, we drop the index  $n$  and the wavevector  $k$  from now on. In bilayer graphene, the two electronic bands near the Dirac point energy exhibit almost identical e-ph coupling strengths [Fig. 1(c)].

The key factors determining the e-ph coupling strength are the density of states around the Dirac point energy and the e-ph matrix elements between the initial and the final electronic states close to the Fermi level. The density of states of pristine graphene vanishes at the Fermi level, whereas bilayer graphene has a finite density of states. Despite this difference, at low doping with only one band occupied ( $|E_F - E_D| < 0.2$  eV,  $E_D$  being the energy at the Dirac point and is set to  $E_D = 0$  in the fol-

lowing discussion), the e-ph coupling strengths in bilayer graphene and in graphite are similar (within 5%) to those of graphene. This indicates that, as in graphene, there is no significant scattering between low-energy electronic states in bilayer graphene and in graphite arising from the e-ph interaction. This behavior originates from the chiral nature of the charge carriers in bilayer graphene<sup>23,24</sup> and in graphite<sup>25</sup>, i.e., it is a matrix-element effect. The difference in the e-ph coupling strength between graphene and bilayer graphene (or graphite) increases with doping. At the largest doping level considered ( $E_F = 1.5$  eV, Figs. 1(c) and 1(d)], the coupling strength in bilayer graphene and graphite ( $\lambda = 0.28$ ) is 30% larger than in graphene ( $\lambda = 0.21$ ). As we show in the following, these differences result from interlayer interaction.

In order to determine which phonon modes lead to the differences in the e-ph coupling strengths between monolayer and bilayer graphene, we decomposed the coupling strength  $\lambda_{nk}$  of both systems into contributions from each phonon branch and wavevector. Figures 2(b) and 2(e) show the Fermi surfaces of hole-doped graphene and bilayer graphene and the initial wavevector  $k$  of the electronic state considered. Figures 2(c) and 2(f) show the phonon dispersions of both pristine and hole-doped graphene and bilayer graphene, respectively. The size of the disks superimposed to the phonon dispersions is proportional to the contribution to the coupling strength  $\lambda_{nk}$  arising from the corresponding phonon mode. Figures 2(c) and 2(f) show that both in graphene and in bilayer graphene, the major contributions result from the highest-energy in-plane vibrations with wavevectors connecting the initial and final electronic states on the Fermi surface. However, in the case of bilayer graphene, the three low-energy optical branches with energy 10 meV enhance the e-ph coupling strength with respect to graphene. The latter vibrations correspond to the compression mode (singly degenerate) and to the sliding mode of the two layers (doubly-degenerate).

Since, as in graphene, the e-ph coupling strength in bilayer graphene is rather small, even in the heavily doped case considered here, it appears unlikely for bilayer graphene to exhibit superconductivity with a transition temperature significantly higher than that one may expect for graphene.

Recent angle-resolved photoemission experiments on kish graphite<sup>26</sup> and on a single crystal of graphite<sup>27</sup> reported very different values of the e-ph renormalization, namely,  $\lambda = 0.70$  along the  $KK$  direction [path indicated by the double-head arrow in Fig. 1(b)]<sup>26</sup> and  $\lambda = 0.14$  along the  $KM$  direction [Fig. 1(b)]<sup>27</sup>. Our calculated e-ph coupling strength in undoped graphite ( $\lambda = 0.034$ ) is closer to the estimate of Ref.<sup>27</sup>. In that work, the broadening of the energy distribution curve in the photoemission spectra was entirely assigned to the e-ph interaction. This assumption leads to an apparent e-ph coupling strength which is enhanced by the contributions arising from other interactions. In particular, it has been shown that the electronic linewidth in graphite

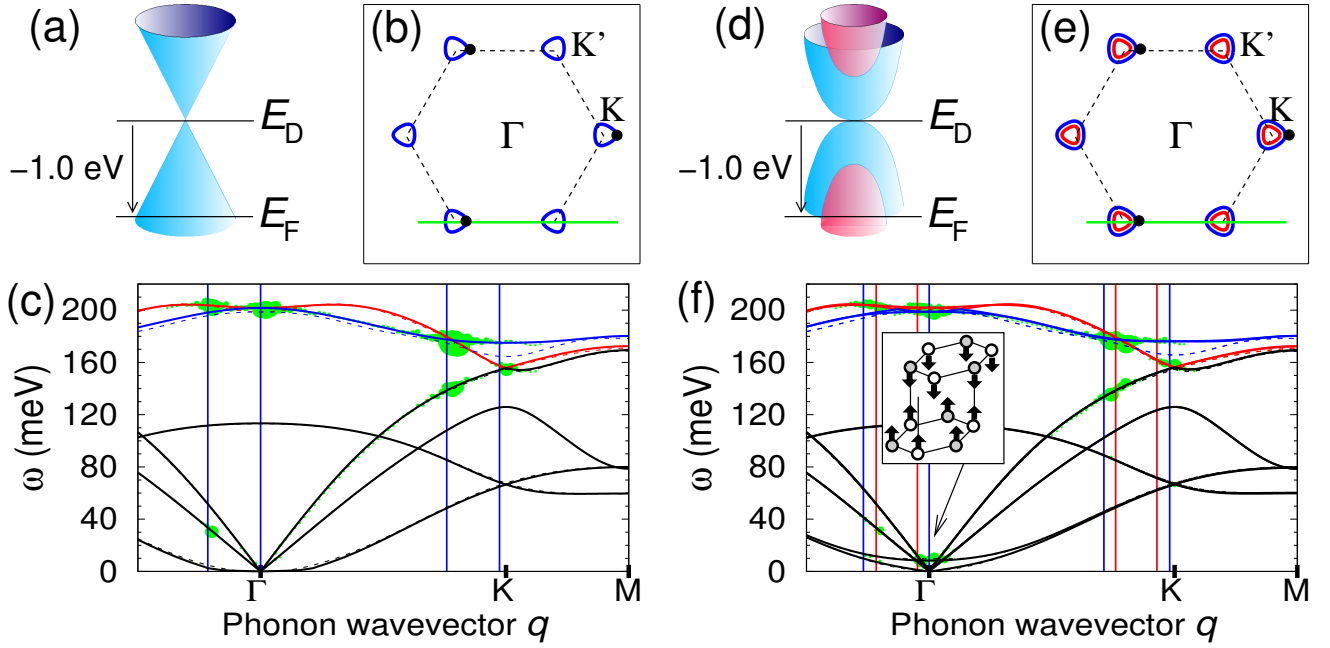


FIG. 2: (a) The electronic energy dispersion and the Fermi level of hole-doped graphene. (b) The Fermi surface (contours) and the Brillouin zone (dashed hexagon) of hole-doped graphene. The black dots represent the wavevector  $k$  of the electronic state considered on the Fermi surface. (c) The phonon dispersion curves of undoped (dashed lines) and hole-doped (solid lines) graphene versus the wavevector  $q$  along the solid green line shown in (b). The vertical lines indicate the phonon wavevectors  $q$  such that the final electronic state with wavevector  $k + q$  is also on the Fermi surface. The size of the disks on top of the phonon dispersions is proportional to the contribution of that phonon mode to  $\chi_{nk}$ . (d) to (f): Same quantities as in (a) to (c) for hole-doped bilayer graphene but including also interband coupling. The inset of (f) shows one of the three modes responsible for the enhancement of the e-ph coupling strength in bilayer graphene. The color (red and blue) and the type (solid and dashed) of the curves in (c) and (f) corresponds to the phonon branches in Figs. 4(a) and 4(b) and 4(c) and 4(d), respectively.

arising from the electron-electron interaction is sizable<sup>28</sup>. A similar discrepancy has been pointed out for the case of graphene<sup>29,30</sup>. However, recent calculations indicate that the effect of the electron-electron interaction in graphene is not negligible and must be taken into account in the analysis of the experimental data<sup>31</sup>.

So far we have discussed the effect of the e-ph interaction on the Fermi velocity of the carriers. In what follows we focus on the effect of e-ph interaction on the phonon linewidths. Figure 3(a) shows the linewidth of the doubly-degenerate  $E_{2g}$  phonons at the  $\Gamma$  point and of the doubly-degenerate  $A_1^0$  mode at the K point for graphene. These phonons exhibit a finite and constant linewidth for  $\mu_F < \mu_{ph} = 2$ , where  $\mu_{ph} = 0.2$  eV is the optical phonon energy, and a negligible linewidth otherwise. The dependence of the phonon linewidth on the doping level can be explained by considering that interband transitions through phonon absorption are forbidden whenever  $\mu_F > \mu_{ph} = 2$ . Our calculated linewidth of the  $E_{2g}$  phonon is in good agreement with previous studies<sup>32,33</sup>.

In bilayer graphene, as a consequence of the interlayer coupling, the four highest-energy modes (originating from the  $E_{2g}$  modes of graphene) split into two sets of doubly-degenerate  $E_g$  and  $E_u$  modes<sup>34</sup>, with the  $E_u$

modes 1.1 meV higher in energy than the  $E_g$  modes (cf. Fig. 3). Interestingly, at  $\Gamma$ , only the  $E_g$  modes exhibit a finite linewidth (1.1 meV) whereas the  $E_u$  modes are not broadened by the e-ph interaction. It can be shown that this difference results from (i) the chiral nature of the low-energy electronic states<sup>25,35</sup> and (ii) from the fact that atoms in the same sublattice but different layers move in phase in the  $E_g$  modes, while they move out of phase in the  $E_u$  modes<sup>36</sup>. The calculated linewidths of the  $E_g$  and the  $E_u$  modes are in good agreement with a previous study based on a pseudospin effective Hamiltonian for the massive Dirac fermions of bilayer graphene<sup>36</sup>.

Among the two sets of high-energy zone-center modes, only the  $E_g$  phonons are Raman active<sup>34</sup>. The calculated phonon linewidth of the  $E_g$  modes can therefore be compared directly with the measured broadening of the Raman lines. As shown in Fig. 3(b), our calculated linewidths are in excellent agreement with those reported in a recent experimental study<sup>37</sup>. For the purpose of comparison, we have downshifted the experimental linewidths of the  $E_{2g}$  phonon in graphene<sup>38</sup> and of the  $E_g$  phonon mode in bilayer graphene<sup>37</sup> by 0.6 meV. The agreement between our calculations and experiment after the subtraction of this uniform background indicates that defect-induced scattering and anharmonic effects are

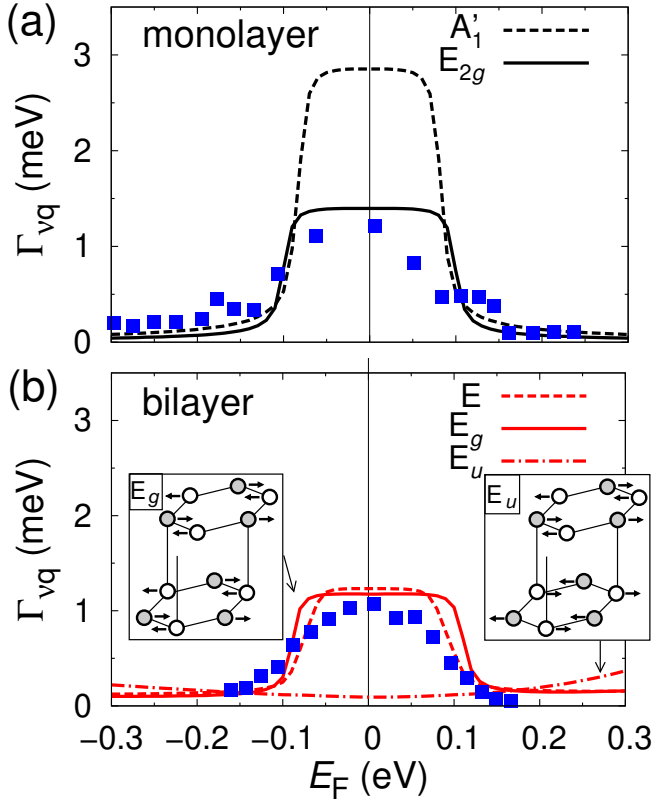


FIG. 3: (a) Phonon linewidth in doped graphene for the  $E_{2g}$  mode at the  $\Gamma$  point (solid line) and the  $A'_1$  mode at the K point (dashed line) versus the Fermi level  $E_F$ . The filled blue squares are the experimental data from Ref.<sup>38</sup> downshifted by 0.6 meV (to account for a uniform background). (b) Phonon linewidth in bilayer graphene for the  $E_g$  mode (solid line) and the  $E_u$  mode (dash-dotted line) at the  $\Gamma$  point, and for the  $E$  mode at the K point (dashed line). The insets show one of each of the two doubly-degenerate zone-center modes considered here. The filled blue squares are the experimental data from Ref.<sup>37</sup> downshifted by 0.6 meV (to account for a uniform background).

small and similar in magnitude in graphene and bilayer graphene.

We note that the linewidth of the  $E_{2g}$  phonons in graphene (1.1 meV) and that of the  $E_g$  phonons in bilayer graphene (1.4 meV) are very similar. This behavior originates from the cancellation of the effects of larger electron density of states and smaller e-ph matrix elements of bilayer graphene as compared to graphene. Because of their similar linewidths, the broadening of these modes is unlikely to be useful for determining the number of graphene layers using Raman spectroscopy. In contrast, the linewidth of the highest-energy mode at the K point in graphene (the  $A'_1$  mode) is reduced from 2.9 meV in graphene to 1.2 meV in bilayer graphene (the  $E$  mode). Therefore it should be possible, at least in principle, to exploit this difference in two-phonon Raman experiments to distinguish between graphene and bilayer graphene.

Figure 4(a) shows the linewidths of the two highest-energy phonon branches in pristine graphene. The phonon linewidths exhibit maxima at the K point and at or near the  $\Gamma$  point. At the  $\Gamma$  point, the highest-energy phonons decay through electronic transitions with no momentum transfer. At the K point, because of the topology of the Dirac cone, non-vertical transitions can occur if the wavevector of the phonon is smaller than  $k_0 = \epsilon_{ph} = v_F$  ( $\epsilon_{ph}$  being the phonon energy and  $v_F$  the Fermi velocity). These transitions are allowed since the phonon wavevectors connect electronic states of the same chirality<sup>39</sup>. The scattering of phonons with wavevector  $k_0 = \epsilon_{ph} = v_F$  is enhanced because the phase velocity of the phonon matches the slope of the Dirac cone. Correspondingly, at this wavevector the transverse-optical phonon branch exhibits the largest linewidth. Unlike the case for the transverse-optical phonons, the longitudinal-optical phonons with wavevector  $k_0$  cannot promote electronic transitions, as a consequence of the chiral symmetry<sup>39</sup>, and the corresponding linewidth vanishes.

As shown in Fig. 4(b), in hole-doped graphene, the phonon linewidths in the highest energy branches with wavevector at the  $\Gamma$  point or at the K point are negligible. However, whenever the phonon wavevector exceeds  $k_0$  in magnitude, intraband electronic transitions can occur through phonon absorption. In the case of phonons with wavevector close to the K point, this kind of electronic transition is suppressed due to chirality<sup>39</sup>. In hole-doped graphene, the Fermi surface consists of two contours centered around the two inequivalent Dirac points. Two maxima are found in the phonon linewidths near K, corresponding to the smallest and the largest wavevectors connecting electronic states on different contours.

Figures 4(c) and 4(d) show the linewidths of the  $E_g$  phonons for undoped as well as for hole-doped ( $E_F = 1.0$  eV) bilayer graphene, respectively. In the undoped case, the linewidths of transverse phonons with wavevector  $k_0$  are not as large as in graphene since the low-energy electronic energy dispersions are nonlinear. In the case of hole-doped bilayer graphene, the profile of the phonon linewidths is almost identical to the one calculated for graphene. This can be explained by considering that the electronic density of states per carbon atom near the Fermi level in graphene and bilayer graphene are very similar.

The results of our calculations could be confirmed by performing detailed inelastic neutron scattering, electron energy loss spectroscopy, or inelastic x-ray scattering experiments. Measurements of this kind have been performed, for example, in the case of magnesium diboride, allowing for a direct comparison with theoretical calculations.<sup>40</sup>

In summary the Fermi velocity renormalization and the phonon line broadening arising from the e-ph interaction in bilayer graphene and in graphite are studied and compared with the corresponding quantities in graphene. In bilayer graphene and in graphite, the e-

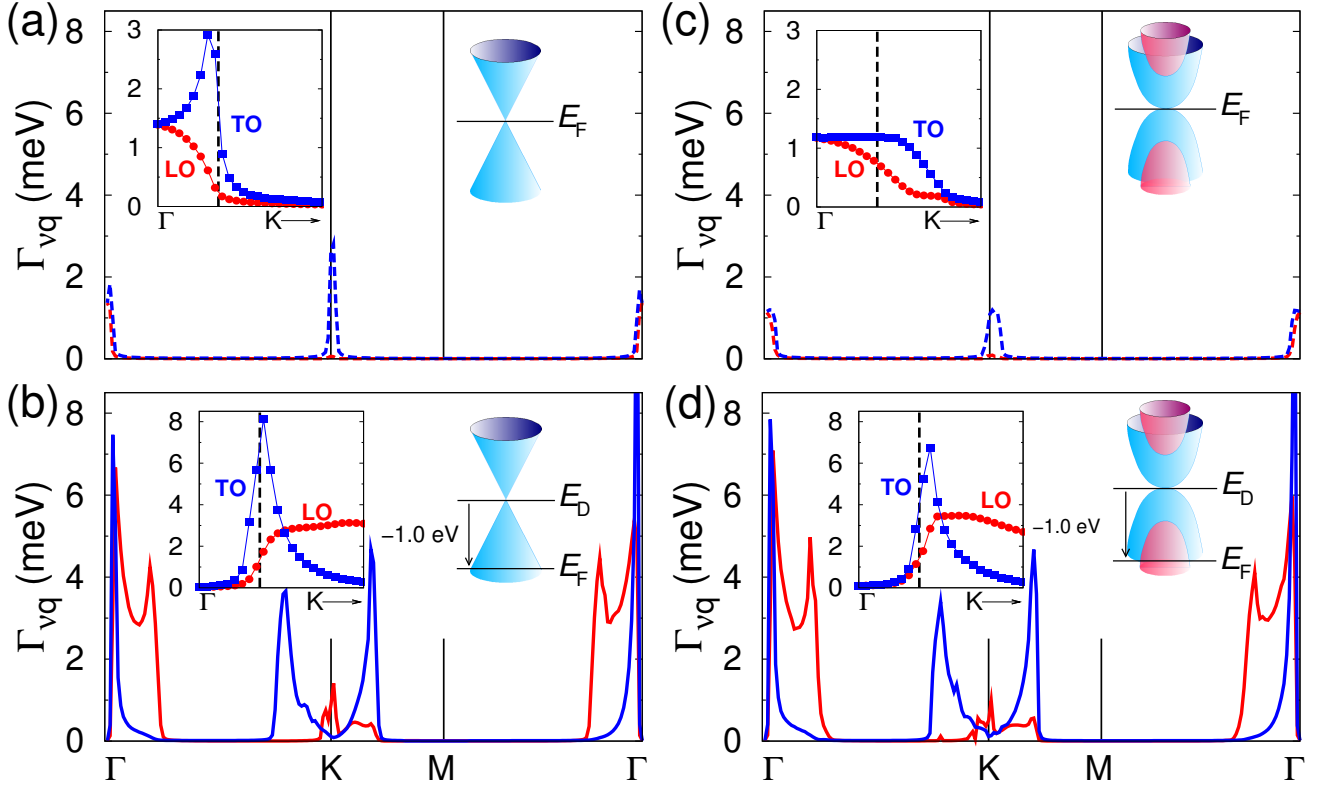


FIG. 4: (a), (b): The phonon linewidth of the highest energy branches in undoped [(a)] and hole-doped [(b)] graphene. The color code (red and blue) and the type (solid and dashed) of the line correspond to the phonon branches shown in Fig. 2(c). (c), (d): Phonon linewidth of the second highest doubly-degenerate phonon branches at the  $\Gamma$  point in undoped [(c)] and hole-doped [(d)] bilayer graphene. The color code (red and blue) and the type (solid and dashed) of the line corresponds to the phonon branches shown in Fig. 2(f). The inset in each panel shows a magnified view of the region near the  $\Gamma$  point, where the symbols represent calculated data points and the lines are a guide to the eye. The vertical dashed line in the inset specifies the characteristic wavevector  $k_0$  (see text).

ph coupling strength is enhanced by up to 30% at high doping as compared to graphene. The calculated doping dependence of the phonon linewidth of the zone-center  $E_g$  mode in bilayer graphene is in excellent agreement with recent Raman measurements<sup>38</sup>. We discussed the similarities and the differences in the linewidths of the optical phonons in graphene and in bilayer graphene.

We thank E. Rotenberg, Jessica L. McChesney, Aaron Bostwick, Michel Côté, Jia-An Yan and Jay Deep Sau for fruitful discussions. This work was supported by NSF Grant No. DMR-07-05941 and by the Director, Office of Science, Office of Basic Energy Sciences, Division of Materials Sciences and Engineering Division, U.S. Department of Energy under Contract No. DE-AC02-

05CH11231. Computational resources have been provided by the National Partnership for Advanced Computational Infrastructure (NPACI) and the National Energy Research Scientific Computing Center (NERSC). Part of the calculations were performed using modified versions of the Quantum-Espresso<sup>41</sup> and the Wannier<sup>42</sup> packages.

**Additions and Corrections.** In this paper [C.-H. Park, F. G. Giustino, M. L. Cohen, and S. G. Louie, *Nano Lett.* **8**, 4229(4233) (2008)], we failed to cite three relevant experimental papers<sup>43,44,45</sup>. These references report on Raman measurements on electrically gated single-layer graphene<sup>43,44</sup> and bilayer graphene<sup>45</sup>.

<sup>Y</sup>Present address: University of Oxford, Department of Materials, Parks Road, OX1 3PH, UK.

Electronic address: cheolwhan@civet.berkeley.edu

<sup>1</sup> K. S. Novoselov, A. K. Geim, S. V. Morozov, D. Jiang, Y. Zhang, S. V. Dubonos, I. V. Grigorieva, and A. A. Firsov, *Science* **306**, 666 (2004).

<sup>2</sup> K. S. Novoselov, D. Jiang, F. Schedin, T. Booth, V. V. Khotkevich, S. V. Morozov, and A. K. Geim, *Proc. Nat.*

*Acad. Sci. U.S.A.* **102**, 10451 (2005).

<sup>3</sup> K. S. Novoselov, A. K. Geim, S. V. Morozov, D. Jiang, M. I. Katsnelson, I. V. Grigorieva, S. V. Dubonos, and F. A. A., *Nature* **438**, 197 (2005).

<sup>4</sup> Y. Zhang, J. W. Tan, H. L. Stormer, and P. Kim, *Nature* **438**, 201 (2005).

- <sup>5</sup> C. Berger, Z. M. Song, X. B. Li, X. S. Wu, N. Brown, C. Naud, T. B. Li, J. Hass, A. N. M. Archenkov, E. H. Conrad, et al., *Science* 312, 1191 (2006).
- <sup>6</sup> A. K. Geim and K. S. Novoselov, *Nature Mater.* 6, 183 (2007).
- <sup>7</sup> S. Engelsberg and J. R. Schrieffer, *Phys. Rev.* 131, 993 (1963), URL <http://link.aip.org/link/?PR/131/993/1>.
- <sup>8</sup> G. Grimvall, *The Electron-Phonon Interaction in Metals* (North-Holland, New York, 1981).
- <sup>9</sup> P. B. Allen and M. L. Cohen, *Phys. Rev. Lett.* 29, 1593 (1972).
- <sup>10</sup> S. G. Louie and M. L. Cohen, eds., *Conceptual Foundations of Materials: A Standard Model for Ground- and Excited-State Properties* (Elsevier, Amsterdam, 2006).
- <sup>11</sup> D. M. Ceperley and B. J. Alder, *Phys. Rev. Lett.* 45, 566 (1980).
- <sup>12</sup> J. P. Perdew and A. Zunger, *Phys. Rev. B* 23, 5048 (1981), URL <http://link.aps.org/abstract/PRB/v23/p5048>.
- <sup>13</sup> S. Baroni, S. de Gironcoli, A. Dal Corso, and P. Giannozzi, *Rev. Mod. Phys.* 73, 515 (2001).
- <sup>14</sup> J. Ihm, A. Zunger, and M. L. Cohen, *J. Phys. C* 12, 4409 (1979).
- <sup>15</sup> N. Troullier and J. L. Martins, *Phys. Rev. B* 43, 1993 (1991).
- <sup>16</sup> M. Fuchs and M. Scheer, *Comput. Phys. Commun.* 119, 67 (1999).
- <sup>17</sup> F. Giustino, J. R. Yates, I. Souza, M. L. Cohen, and S. G. Louie, *Phys. Rev. Lett.* 98, 047005 (pages 4) (2007), URL <http://link.aps.org/abstract/PRL/v98/e047005>.
- <sup>18</sup> F. Giustino, M. L. Cohen, and S. G. Louie, *Phys. Rev. B* 76, 165108 (2007).
- <sup>19</sup> N. Marzari and D. Vanderbilt, *Phys. Rev. B* 56, 12847 (1997).
- <sup>20</sup> I. Souza, N. Marzari, and D. Vanderbilt, *Phys. Rev. B* 65, 035109 (2001).
- <sup>21</sup> The relaxed nearest neighbor carbon-carbon distances [ $b$  in Fig. 1(a)] for pristine graphene, bilayer graphene, and graphite are 1.40 Å, 1.40 Å, and 1.42 Å, respectively. The interlayer distances [ $d$  in Fig. 1(a)] for bilayer graphene and for graphite are 3.21 Å and 3.26 Å, respectively. The relaxed lattice parameters for monolayer graphene and for graphite are in good agreement with previous calculations<sup>46</sup> as well as with experiments<sup>47,48</sup>.
- <sup>22</sup> C.-H. Park, F. Giustino, J. L. McChesney, A. Bostwick, T. Ohta, E. Rotenberg, M. L. Cohen, and S. G. Louie, *Phys. Rev. B* 77, 113410 (2008).
- <sup>23</sup> E. McCann and V. I. Fal'ko, *Phys. Rev. Lett.* 96, 086805 (2006).
- <sup>24</sup> M. I. Katsnelson, K. S. Novoselov, and A. K. Geim, *Nature Phys.* 2, 620 (2006).
- <sup>25</sup> P. R. Wallace, *Phys. Rev.* 71, 622 (1947).
- <sup>26</sup> K. Sugawara, T. Sato, S. Souma, T. Takahashi, and H. Suenomatsu, *Phys. Rev. Lett.* 98, 036801 (2007).
- <sup>27</sup> C. S. Leem, B. J. Kim, C. Kim, S. R. Park, T. Ohta, A. Bostwick, E. Rotenberg, H. D. Kim, M. K. Kim, H. J. Choi, et al., *Phys. Rev. Lett.* 100, 016802 (2008).
- <sup>28</sup> C. D. Spataru, M. A. Cazalilla, A. Rubio, L. X. Benedict, P. M. Echenique, and S. G. Louie, *Phys. Rev. Lett.* 87, 246405 (2001).
- <sup>29</sup> A. G. Runeis, C. Attaccalite, A. Rubio, D. Vyalikh, S. L. Molodtsov, J. Fink, R. Follath, W. Eberhardt, B. Buchner, and T. Pichler, *arXiv:0808.1613v1*.
- <sup>30</sup> J. L. McChesney, A. Bostwick, T. Ohta, K. Emtsev, T. Seyller, K. Homa, and E. Rotenberg, *arXiv:0809.4046v1*.
- <sup>31</sup> C.-H. Park, F. Giustino, C. D. Spataru, M. L. Cohen, and S. G. Louie, unpublished.
- <sup>32</sup> T. Ando, *J. Phys. Soc. Jpn.* 75, 124701 (2006).
- <sup>33</sup> M. Lazzeri and F. Mauri, *Phys. Rev. Lett.* 97, 266407 (pages 4) (2006).
- <sup>34</sup> J.-A. Yan, W. Y. Ruan, and M. Y. Chou, *Phys. Rev. B* 77, 125401 (2008).
- <sup>35</sup> T. Ando, *J. Phys. Soc. Jpn.* 74, 777 (2005).
- <sup>36</sup> T. Ando, *J. Phys. Soc. Jpn.* 76, 104711 (2007).
- <sup>37</sup> J. Yan, E. A. Henriksen, P. Kim, and A. Pinczuk, *Phys. Rev. Lett.* 101, 136804 (2008).
- <sup>38</sup> J. Yan, Y. Zhang, P. Kim, and A. Pinczuk, *Phys. Rev. Lett.* 98, 166802 (pages 4) (2007).
- <sup>39</sup> S. Piscanec, M. Lazzeri, F. Mauri, A. C. Ferrari, and J. Robertson, *Phys. Rev. Lett.* 93, 185503 (2004).
- <sup>40</sup> A. Shukla, M. Calandra, M. d'Astuto, M. Lazzeri, F. Mauri, C. Bellin, M. K. Kirsch, J. Karpinski, S. M. Kazakov, J. Jun, et al., *Phys. Rev. Lett.* 90, 095506 (2003).
- <sup>41</sup> S. Baroni, S. de Gironcoli, A. D. Corso, P. Giannozzi, and F. Mauri, computer code Quantum-Espresso, 2006, <http://www.quantum-espresso.org>.
- <sup>42</sup> A. Mosto, J. R. Yates, Y.-S. Lee, I. Souza, D. Vanderbilt, and N. Marzari, computer code Wannier90, 2007, <http://www.wannier.org>.
- <sup>43</sup> S. Pisana, M. Lazzeri, C. Casiraghi, K. S. Novoselov, A. K. Geim, A. C. Ferrari, and F. Mauri, *Nat. Mater.* 6, 198 (2007).
- <sup>44</sup> A. Das, S. Pisana, B. Chakraborty, S. Piscanec, S. K. Saha, U. V. Waghmare, K. S. Novoselov, H. R. Krishnamurthy, A. K. Geim, A. C. Ferrari, et al., *Nat. Nano* 3, 210 (2008).
- <sup>45</sup> A. Das, B. Chakraborty, S. Piscanec, S. Pisana, A. K. Sood, and A. C. Ferrari, *arXiv:0807.1631v1*.
- <sup>46</sup> N. Mounet and N. Marzari, *Phys. Rev. B* 71, 205214 (pages 14) (2005).
- <sup>47</sup> Y. X. Zhao and I. L. Spain, *Phys. Rev. B* 40, 993 (1989).
- <sup>48</sup> M. Han and H. Beister, and K. Syassen, *Phys. Rev. B* 39, 12598 (1989).